Absorber and emitter for solar thermo-photovoltaic systems to achieve efficiency exceeding the Shockley-Queisser limit

Eden Rephaeli[1,*] and Shanhui Fan[2]

[1]*Department of Applied Physics, Stanford University, Stanford, California, 94305, USA*
[2]*Department of Electrical Engineering, Stanford University, Stanford, California, 94305, USA*
**edenr@stanford.edu*

Abstract: We present theoretical considerations as well as detailed numerical design of absorber and emitter for Solar Thermophotovoltaics (STPV) applications. The absorber, consisting of an array of tungsten pyramids, was designed to provide near-unity absorptivity over all solar wavelengths for a wide angular range, enabling it to absorb light effectively from solar sources regardless of concentration. The emitter, a tungsten slab with Si/SiO_2 multilayer stack, provides a sharp emissivity peak at the solar cell band-gap while suppressing emission at lower frequencies. We show that, under a suitable light concentration condition, and with a reasonable area ratio between the emitter and absorber, a STPV system employing such absorber-emitter pair and a single-junction solar cell can attain efficiency that exceeds the Shockley-Queisser limit.

OCIS codes: (350.6050) Solar energy; (350.4238) Nanophotonics and photonic crystals

References and links

1. W. Shockley, and H. J. Queisser, "Detailed Balance Limit of Efficiency of p-n Junction Solar Cells," J. Appl. Phys. **32**(3), 510–519 (1961).
2. R. M. Swanson, "A proposed thermophotovoltaic solar energy conversion system," Proc. IEEE **67**(3), 446–447 (1979).
3. W. Ruppel, and P. Wurfel, "Upper limit for the conversion of solar energy," IEEE Trans. Electron. Dev. **27**(4), 877–882 (1980).
4. W. Spirkl, and H. Ries, "Solar thermophotovoltaics: An assessment," J. Appl. Phys. **57**(9), 4409–4414 (1985).
5. P. T. Landsberg, and P. Baruch, "The thermodynamics of the conversion of radiation energy for photovoltaics," J. Phys. Math. Gen. **22**(11), 1911–1926 (1989).
6. T. K. Chaudhuri, "A solar thermophotovoltaic converter using Pbs photovoltaic cells," Int. J. Energy Res. **16**(6), 481–487 (1992).
7. V. Badescu, "Thermodynamic theory of thermophotovoltaic solar energy conversion," J. Appl. Phys. **90**(12), 6476–6486 (2001).
8. V. Badescu, "Upper bounds for solar thermophotovoltaic efficiency," Renew. Energy **30**(2), 211–225 (2005).
9. N. P. Harder, and P. Wurfel, "Theoretical limits of thermophotovoltaic solar energy conversion," Semicond. Sci. Technol. **18**(5), S151–S157 (2003).
10. I. Tobias, and A. Luque, "Ideal efficiency and potential of solar thermophotonic converters under optically and thermally concentrated power flux," IEEE Trans. Electron. Dev. **49**(11), 2024–2030 (2002).
11. M. Florescu, H. Lee, I. Puscasu, M. Pralle, L. Florescu, D. Z. Ting, and J. P. Dowling, "Improving solar cell efficiency using photonic band-gap materials," Sol. Energy Mater. Sol. Cells **91**, 1599–1610 (2007).
12. A. S. Vlasov, V. P. Khvostikov, O. A. Khvostikova, P. Y. Gazaryan, S. V. Sorokina, and V. M. Andreev, "TPV Systems with Solar Powered Tungsten Emitters," AIP Conf. Proc. **890**, 327–334 (2007).
13. V. M. Andreev, V. P. Khvostikov, O. A. Khvostikova, A. S. Vlasov, P. Y. Gazaryan, N. A. Sadchikov, and V. D. Rumyantsev, Solar thermophotovoltaic system with high temperature tungsten emitter," in *Photovoltaic Specialists Conference, 2005. Conference Record of the Thirty-first IEEE* (2005), pp. 671–674.
14. K. W. Stone, N. S. Fatemi, and L. M. Garverick, "Operation and component testing of a solar thermophotovoltaic power system," in *Photovoltaic Specialists Conference, 1996, Conference Record of the Twenty Fifth IEEE* (1996), pp. 1421–1424.

#112945 - $15.00 USD Received 16 Jun 2009; revised 20 Jul 2009; accepted 20 Jul 2009; published 11 Aug 2009

15. H. Yugami, H. Sai, K. Nakamura, N. Nakagawa, and H. Ohtsubo, "Solar thermophotovoltaic using $Al_2O_3Er_3Al_5O_{12}$ eutectic composite selective emitter," in *Photovoltaic Specialists Conference, 2000. Conference Record of the Twenty-Eighth IEEE* (2000), pp. 1214–1217.
16. D. L. Chan, M. Soljacić, and J. D. Joannopoulos, "Thermal emission and design in 2D-periodic metallic photonic crystal slabs," Opt. Express **14**(19), 8785–8796 (2006).
17. E. Rephaeli, and S. Fan, "Tungsten black absorber for solar light with wide angular operation range," Appl. Phys. Lett. **92**(21), 211107 (2008).
18. Y. B. Chen, and Z. M. Zhang, "Design of tungsten complex gratings for thermophotovoltaic radiators," Opt. Commun. **269**(2), 411–417 (2007).
19. A. Heinzel, V. Boerner, A. Gombert, B. Blasi, V. Wittwer, and J. Luther, "Radiation filters and emitters for the NIR based on periodically structured metal surfaces," J. Mod. Opt. **47**, 2399–2419 (2000).
20. I. Celanovic, N. Jovanovic, and J. Kassakian, "Two-dimensional tungsten photonic crystals as selective thermal emitters," Appl. Phys. Lett. **92**(19), 193101 (2008).
21. H. Sai, and H. Yugami, "Thermophotovoltaic generation with selective radiators based on tungsten surface gratings," Appl. Phys. Lett. **85**(16), 3399 (2004).
22. S. Y. Lin, J. Moreno, and J. G. Fleming, "Three-dimensional photonic-crystal emitter for thermal photovoltaic power generation," Appl. Phys. Lett. **83**(2), 380 (2003).
23. A. Narayanaswamy, and G. Chen, "Thermal emission control with one-dimensional metallodielectric photonic crystals," Phys. Rev. B **70**(12), 125101 (2004).
24. I. Celanovic, D. Perreault, and J. Kassakian, "Resonant-cavity enhanced thermal emission," Phys. Rev. B **72**(7), 075127 (2005).
25. Y. Fink, J. N. Winn, S. Fan, C. Chen, J. Michel, J. D. Joannopoulos, and E. L. Thomas, "A dielectric omnidirectional reflector," Science **282**(5394), 1679–1682 (1998).
26. S. G. Tikhodeev, A. L. Yablonskii, E. A. Muljarov, N. A. Gippius, and T. Ishihara, "Quasiguided modes and optical properties of photonic crystal slabs," Phys. Rev. B **66**(4), 045102 (2002).
27. E. D. Palik, *Handbook of Optical Constants of Solids,* (Academic, New York, 1985).

1. Introduction

When a single-junction solar cell is illuminated by sunlight, its efficiency is subject to the Shockley-Queisser (SQ) limit [1], which sets a fundamental upper bound on its efficiency. This limit arises from several intrinsic loss mechanisms: Solar photons below the band-gap do not contribute to electrical current. For each photon above the band-gap, the difference between the photon energy, and the output energy at somewhat below the band-gap energy is dissipated as heat. As a result, the theoretical maximum efficiency [1] of an ideal single-junction cell maintained at a room temperature of 300K cannot exceed 41% under solar illumination and maximum concentration. In the absence of concentration this limit is 31%.

Solar Thermophotovolatics (STPV) seeks to overcome the SQ limit through the use of an intermediate structure that absorbs the suns' rays, heats up, and emits towards a solar cell a narrow-banded spectrum directly above the band-gap of the solar cell [2–15] (Fig. 1(a)). Using a single junction cell, this scenario has been shown [9] to achieve theoretical efficiencies of up to 54% and 85%, in the absence of concentration and full concentration of light, respectively. A number of solar TPV systems have been realized experimentally [13–15].

#112945 - $15.00 USD Received 16 Jun 2009; revised 20 Jul 2009; accepted 20 Jul 2009; published 11 Aug 2009

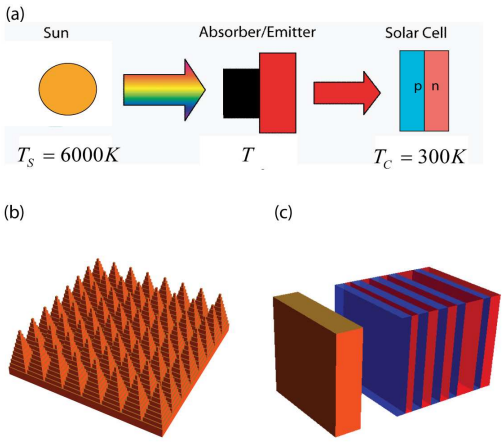

Fig. 1. (a) Schematic of STPV system. (b) Illustration of tungsten pyramid absorber (period: 250nm, height: 500nm.) (c) Illustration of tungsten slab emitter, including 10 layers of alternating Si / SiO_2. Layer thicknesses, beginning with the air gap, and in the unit of μm are: [0.771, **0.193**, 0.145, **0.219**, 0.215, **0.218**, 0.210, **0.198**, 0.426, **0.178**, 0.249]. Blue indicates Si, red indicates SiO_2

The efficiency gain of STPV arises entirely from the use of the intermediate structure that consists of an absorber and emitter pair. However, to date no realistic design has been put forth for an appropriate intermediate structure that, when used in a STPV system with a single-junction solar cell, allows theoretical efficiencies that exceed the SQ limit. In [13], a STPV system with a tungsten emitter and GaSb solar cells was tested. The system showed a ~10% overall (experimental) efficiency with the use of unstructured Tungsten emitters at a concentration of 4000 suns. In addition the authors also performed theoretical efficiency calculations obtaining ~11.5% efficiency with a 0.7[eV] cell. When using a 3D photonic crystal emitter from reference [16] with the additional assumption of 90% recycling of sub-band-gap photons and concentration of 8000 suns, the overall efficiency was calculated as ~30-32%. In comparison, the SQ limit for a 0.7[eV] cell is 36%.

In this paper, we propose a detailed design of a highly efficient intermediate intended for a $E_g = 0.7[eV]$ solar cell. Its absorber, as shown in Fig. 1(b), consists of a tungsten pyramid array [17], closely mimicking the properties of a black absorber at solar wavelengths. Its emitter, as shown in Fig. 1(c), is formed by placing a multilayer Si / SiO_2 dielectric stack near a bare tungsten slab in a configuration which provides both emissivity enhancement at the solar cell band-gap, and emissivity suppression at lower photon energies, compared to an unstructured slab. When integrated into a STPV setup, we show that the composite system can surpass maximum theoretical efficiency of any single-junction solar cell in the SQ limit, even without taking into account the additional efficiency gain due to photon recycling between the emitter and the cell.

In general, the efficiency of a solar TPV system is the product of the efficiencies of the intermediate (η_I) and the solar cell (η_{SC}). The efficiency of the intermediate is defined as the ratio of outgoing power from the emitter with respect to the incoming solar power. The solar cell efficiency (η_{SC}) is defined as the ratio of electrical power extracted from the cell to the incident power radiated by the emitter. As it turns out, these two efficiencies can be discussed somewhat independently, with η_I controlled by the property of the absorber, and

#112945 - $15.00 USD Received 16 Jun 2009; revised 20 Jul 2009; accepted 20 Jul 2009; published 11 Aug 2009

η_{SC} controlled by the property of the emitter. Therefore, the paper is organized as follows: In section 2 we present an analysis of the intermediate efficiency (η_I), as well as the design of an absorber guided by such analysis. In section 3 we then present an analysis of the efficiency of a solar cell (η_{SC}) when illuminated by an emitter. Such an analysis highlights the requirements on the emitter, which we will use in our actual emitter design. The combination of the analyses in section 2 and 3 also results in a computational tool that allows one to evaluate the overall system efficiency $(\eta_I \eta_{SC})$ given realistic spectral information of the emitter and absorber. Using this tool, in section 4 we present analysis of our systems efficiency.

2. Analysis of intermediate efficiency and absorber design

2.1 Intermediate efficiency

We consider an intermediate with an absorber area A_a and emitter area A_e. (For later use we will define an *area ratio* $\beta = A_e / A_a$). Assuming the intermediate is in thermal equilibrium at a temperature T, the incoming and outgoing power must be equal. Further ignoring any radiation from the solar cell to the emitter, we then obtain:

$$A_a\left[J_s(N_s) - J_a(T)\right] = A_e J_e(T) \tag{1}$$

The term $J_s(N_s)$ in Eq. (1), defined as

$$J_s(N_s) = \int_0^{2\pi} d\varphi \int_0^{\theta_C} d\theta \sin\theta\cos\theta \int_0^{\infty} dE\varepsilon_a(E,\theta,\varphi) I_s(E) \tag{2}$$

is the solar irradiance that is incident upon the absorber. Here, $\varepsilon_a(E,\theta,\varphi)$ is the absorptivity of the absorber, averaged over both polarizations. $I_s(E)$ is the solar spectral radiance, in the subsequent calculations we will either use the AM1.5 solar spectrum $I_{AM1.5}(E)$, or a blackbody spectrum $I_{BB}(E,T_s)$ with a solar temperature $T_S = 6000K$. $\theta_C = \sin^{-1}\left(\sqrt{\frac{N_s\Omega_s}{\pi}}\right)$ is related to the number of suns (N_s) that are concentrated, with $\Omega_s = 68.5\mu Sr$ being the solid angle subtended by the sun. A practical STPV system will almost certainly employ light concentration to increase the angular input incident upon the absorber, in order to attain a high enough equilibrium temperature to drive the emitter.

The term $J_a(T)$ in Eq. (1) is defined as

$$J_a(T) = \int_0^{2\pi} d\varphi \int_0^{\pi/2} d\theta \sin(\theta)\cos(\theta) \int_0^{\infty} dE\varepsilon_a(E,\theta,\varphi) I_{BB}(E,T) \tag{3}$$

It is the emitted thermal irradiance from the absorber, with $I_{BB}(E,T)$ being the blackbody spectral radiance at temperature T. The term $J_e(T)$ in Eq. (1), defined as

$$J_e(T) = \int_0^{2\pi} d\varphi \int_0^{\pi/2} d\theta \sin(\theta)\cos(\theta) \int_0^{\infty} dE\varepsilon_e(E,\theta,\varphi) I_{BB}(E,T) \tag{4}$$

#112945 - $15.00 USD Received 16 Jun 2009; revised 20 Jul 2009; accepted 20 Jul 2009; published 11 Aug 2009

is the emitted thermal irradiance from the emitter, with $\varepsilon_e(E,\theta,\varphi)$ being the emissivity of the emitter, averaged over both polarizations. The emitter presented in this paper has emissivity independent of the azimuthal angle φ due to its spatial symmetry.

To determine the intermediate efficiency of a given intermediate exposed to solar light at a particular concentration, we solve Eq. (1) for the equilibrium temperature T of the intermediate. The efficiency of the intermediate is then

$$\eta_I = \frac{A_e}{A_a}\frac{J_e}{J_s} = \beta\frac{J_e}{J_s} \tag{5}$$

We can understand some of the behaviors of η_I by noting that from Eq. (1):

$$\eta_I = \frac{J_s - J_a}{J_s} = 1 - \frac{J_a}{J_s} \tag{6}$$

Thus, the property of the emitter enters only through setting the equilibrium temperature T of the intermediate. Or equivalently, at a given equilibrium temperature T, the behavior of the intermediate efficiency is determined by the absorber only. This observation allows one to discuss the properties of absorber and emitter separately, as we do in this paper. In the case of an ideal solar spectrum with temperature T_S and a blackbody absorber one obtains the intermediate efficiency η_I^{BB} [9]:

$$\eta_I^{BB}(T,N_s) = 1 - \frac{\pi T^4}{N_s\Omega_s T_s^4} \tag{7}$$

In this case the intermediate efficiency is a monotonically decreasing (increasing) function of $T,(N_S)$. Equation (7) is plotted in Fig. 2(a), which will be used to compare to real absorber structures that we will evaluate.

#112945 - $15.00 USD Received 16 Jun 2009; revised 20 Jul 2009; accepted 20 Jul 2009; published 11 Aug 2009

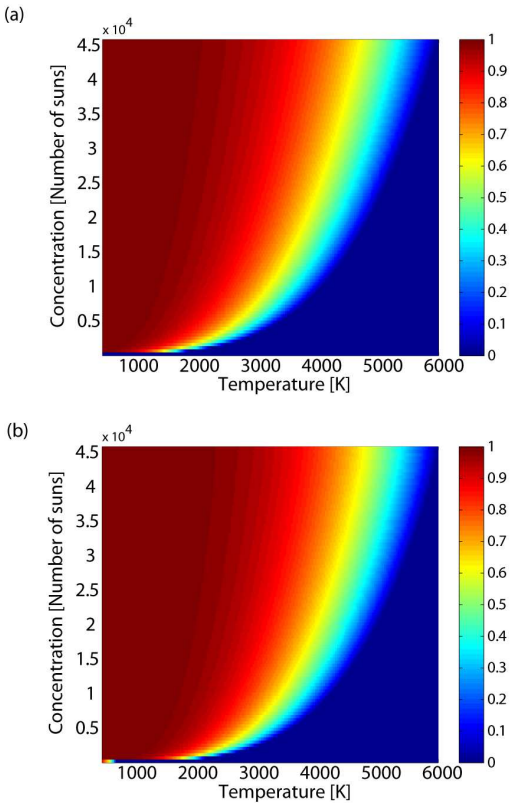

Fig. 2. Intermediate efficiency (η_i) vs. solar concentration (Ns) and equilibrium temperature (T) for: (a) Blackbody absorber. (b) Pyramid array absorber in Fig. 1(b), assuming an ideal solar spectrum with the solar temperature set at 6000K.

2.2 Absorber design

Before we discuss the details of our absorber design we briefly review the basic requirement for absorbers in STPV [9]. While interesting theoretical ideas do exist for designing absorbers that operate in unconcentrated systems [3,9], in practice all demonstrated STPV systems employ sunlight concentration. Therefore, here we focus on designing absorbers for concentrated light, in which case the absorber will need to absorb sunlight over the entire solar spectrum, and over a substantial range of incidence angles.

In addition to the optical properties outlined above, from a material perspective, the absorber needs to withstand fairly high temperatures (typically 1000-2500K), and have high optical loss (which, by proper design can lead to high absorption). The combination of a high melting point of ~3700K and large loss in the optical regime [17] makes tungsten a natural candidate for the absorber material. Previously [17], we presented a design of a tungsten absorber consisting of a square array of pyramids (Fig. 1(b)). The period of the array is 250nm and the height of the pyramid is 500nm. As can be seen by its absorptivity spectrum for normally incident light (Fig. 3(a)), such an absorber closely mimics a blackbody at $\lambda < 2\mu m$, while its absorptivity is greatly reduced at longer wavelengths of $\lambda > 2\mu m$. Moreover, this absorber is also very efficient over a wide range of incidence angle. In Fig. 3(b) we plot the absorber efficiency as a function of concentration. (The absorber efficiency is defined as the fraction of absorbed power for the entire incident solar spectrum at a given concentration). The absorber efficiency is above 95% for most of the concentration condition for the AM1.5 spectrum.

#112945 - $15.00 USD Received 16 Jun 2009; revised 20 Jul 2009; accepted 20 Jul 2009; published 11 Aug 2009

Using our absorber we plot in Fig. 2(b) the intermediate efficiency $\eta_I(T,N_S)$ as a function of temperature and solar concentration. We note that $\eta_I(T,N_S)$ has very similar characteristics as compared to the efficiency $\eta_I^{BB}(T,N_S)$ for an intermediate with an ideal blackbody absorber, as shown in Fig. 2(a). In fact, the pyramid absorber is preferable to an ideal black body absorber. There is very little power in the solar spectrum at the wavelength range longer than $2\mu m$. Thus, the cutoff at $\lambda = 2\mu m$ in the spectrum of our absorber is beneficial in suppressing absorber radiation in the spectral region outside the solar spectrum. As a result, the use of our designed pyramid array absorber can achieve high intermediate efficiency over a wider region of operating conditions. Alternatively, for a given emitter, the use of our designed absorber should result in higher equilibrium temperature compared with the use of a blackbody absorber.

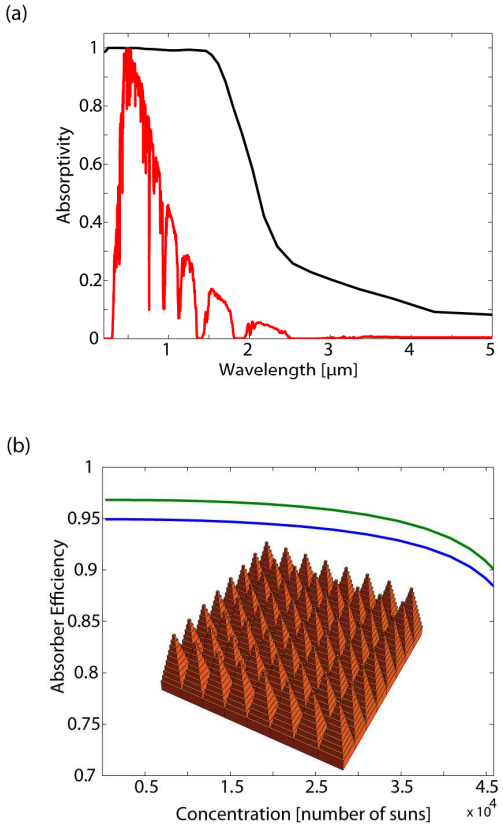

Fig. 3. (a) Absorptivity of tungsten pyramid absorber at normal incidence (red curve), and scaled Atomic Mass 1.5 spectral radiance (gray curve). (b) Absorber efficiency of tungsten pyramid absorber vs. concentration, for the case of an ideal blackbody spectral radiance at 6000K (blue curve), and Atomic Mass 1.5 spectral radiance (green curve).

3. Solar cell efficiency and emitter design

In a STPV system the efficiency of the solar cell is determined by the property of the emitter. Therefore, in this section we will start by presenting an analysis of a solar cell efficiency assuming an incident radiation spectrum. Using this analysis, we then discuss the requirements on the emitter, which leads to our emitter design.

#112945 - $15.00 USD Received 16 Jun 2009; revised 20 Jul 2009; accepted 20 Jul 2009; published 11 Aug 2009

3.1 Solar cell efficiency

As mentioned above, our analysis does not include photon recycling. In the photon recycling process, photons that are not absorbed by or are re-emitted from the solar cell, return to the emitter and are re-absorbed. This process, which plays no role in the original SQ analysis, where a solar cell is directly exposed to the sunlight, is known to have substantial benefits [9,13]. Complete recycling of sub-band-gap photons effectively provides a sharp cut-off of emitter emissivity right at the solar-cell band-gap energy. Complete recycling of re-emitted photons, which are above band-gap, allows one to operate the cell with at a voltage close to the open circuit voltage [9]. Both effects increase the efficiency of the overall STPV system.

However, in practice it is generally difficult to achieve complete recycling of photons. Complete recycling of sub-band-gap photons requires solar-cell materials to have low material loss immediately below the band-gap energy. Complete recycling of the re-emitted photons requires a solar cell that is mostly radiative, where electron-hole pairs recombine mostly through radiative rather than non-radiative processes. In such solar cells, if the energy of an electron-hole pair is not delivered to the external circuit, the pair will recombine radiatively, emits a photon that can then be returned to the emitter without energy loss. Both of these recycling processes are difficult to achieve with high efficiency. In this paper, we will therefore perform a strict SQ analysis, without the added benefit of photon recycling. In this respect, our analysis provides a lower-bound on STPV efficiency. As we will see below, even in this case our design of absorber/emitter pair enables efficiency beyond the theoretical limit of single-junction cell directly exposed to sun light.

The solar cell efficiency (η_{SC}) is defined as the ratio of electrical power extracted from the cell to the incident power radiated by the emitter. According to the SQ analysis, the detailed balance limit of solar cell efficiency η_{sc} consists of three parts

$$\eta_{SC} = U\left(T, E_g\right)\upsilon\left(T, E_g\right)m\left(V_{op}\right) \tag{8}$$

The first term in Eq. (8) is the *ultimate efficiency*. In obtaining the ultimate efficiency one assumes that every photon incident upon the solar cell with $E \geq E_g$ excites an electron-hole pair with band-gap voltage $V_g = E_g / q$, with q denoting an electron's charge. The ultimate efficiency then measures power as contained in excited electron-hole pairs with respect to the incident power:

$$U\left(T, E_g\right) = \frac{\int_0^{\pi/2} d\theta \sin\left(2\theta\right) \int_{E_g}^{\infty} \frac{E_g dE}{E} \varepsilon_e\left(E,\theta\right) I_{BB}\left(E,T\right)}{\int_0^{\pi/2} d\theta \sin\left(2\theta\right) \int_0^{\infty} dE \varepsilon_e\left(E,\theta\right) I_{BB}\left(E,T\right)} \tag{9}$$

The actual efficiency of a SQ cell is reduced from the ultimate efficiency by the second and third factors in Eq. (8). The second factor in Eq. (8) arises since the open-circuit voltage is smaller than the band-gap voltage, V_g, by a factor:

$$\upsilon\left(E_g, T\right) = \frac{V_{op}}{V_g} = \frac{V_C}{V_g} \ln\left(f \frac{Q_e\left(T, E_g\right)}{Q_c\left(T_c, E_g\right)} \right) \tag{10}$$

Here $V_C = k_B T_c / q$ is related to the cell temperature T_c,

#112945 - $15.00 USD Received 16 Jun 2009; revised 20 Jul 2009; accepted 20 Jul 2009; published 11 Aug 2009

$$Q_e\left(T,E_g\right)=\frac{2\pi}{h^3c^2}\int_0^{\pi/2}\sin\left(2\theta\right)d\theta\int_{E_g}^{\infty}\varepsilon_e\left(E,\theta\right)\frac{E^2dE}{\exp\left(E/k_BT\right)-1} \tag{11}$$

is the photon number flux incident on the cell coming from the emitter.

$$Q_c\left(T_c,E_g\right)=\frac{2\pi}{h^3c^2}\int_{E_g}^{\infty}\frac{E^2dE}{\exp\left(E/k_BT_c\right)-1} \tag{12}$$

is the photon number flux incident on the cell when it is surrounded by a blackbody at the temperature of the cell T_c. $f=\frac{f_ct_e}{2t_c}$ is a non-ideality factor that combines the effect of non-radiative recombination $\left(f_c\right)$, the possibility of non-unity absorption coefficient of photon by the cell coming from the emitter $\left(t_e\right)$ and surrounding environment at 300K $\left(t_c\right)$. In this paper, we assume an ideal solar cell with a planar geometry for both the emitter and the cell, hence $f=1/2$. The third factor in Eq. (8), $m\left(V_{op}\right)$, is the impedance matching factor. This factor comes about by a choice of the operating voltage $V_{\max}$ that maximizes the electrical power extracted from the cell, and takes the form:

$$m\left(V_{op}\right)=\frac{z_m^2}{\left(1+z_m-e^{-z_m}\right)\left(z_m+\ln\left(1+z_m\right)\right)} \tag{13}$$

Here $z_m=V_{\max}/V_C$. z_m is related to $z_{op}=V_{op}/V_C$

$$z_{op}=z_m+\ln\left(1+z_m\right) \tag{14}$$

Below, we will use Eqs. (8)-(14) to calculate the efficiency of a 0.7[eV] cell that is exposed to radiation from an emitter.

3.2 Emitter design requirements

Based on the efficiency analysis above, we now discuss the requirement on the emitter. By examining the form of the ultimate efficiency term, $U\left(T,E_g\right)$, we note that an ideal emitter obviously needs to completely suppress sub-band-gap radiation, while restricting the bandwidth of the emission above the band-gap. However, since equilibrium temperatures of the emitter in practical STPV systems are $<2500K$, whereas a typical solar cell has a band-gap energy of 0.7[eV] or greater, the spectral radiance of the incident emission falls off sharply above the band-gap, and becomes negligible at $E>2eV$. As a result, sub-band-gap emission from the emitter represents a bigger detriment than the thermalization loss that results from the emission above the band-gap. Thus, in emitter design it is paramount to cut-off sub-band-gap radiation.

Assuming an emitter with no sub-band-gap radiation we now discuss the effect of varying the bandwidth of emitter radiation. In general, the ultimate efficiency improves as the emitter bandwidth decreases, due to the suppression of thermalization losses. However, the open-circuit voltage V_{op} of the cell and hence the factor $\upsilon\left(T,E_g\right)$ in Eq. (10) monotonically increases as a function of the charge carrier density. Moreover, the impedance matching factor, $m\left(V_{op}\right)$ in Eq. (13), is a monotonically increasing function of open-circuit voltage V_{op} –Hence it too increases with the density of excited charge carriers. Since the charge

#112945 - $15.00 USD Received 16 Jun 2009; revised 20 Jul 2009; accepted 20 Jul 2009; published 11 Aug 2009

carrier density is directly proportional to the total flux of above-band-gap photons that the emitter radiates, reducing the emitter bandwidth reduces open circuit voltage and the impedance matching factor.

To gain further insight, consider a model narrow-band emitter with emissivity:

$$\varepsilon_{ideal}\left(\Delta E\right)=\begin{cases}1;\ E_g < E < E_g+\Delta E\\ 0;\ \text{everywhere else}\end{cases} \tag{15}$$

Here ΔE is the bandwidth of the emitter. In Fig. 4, the three components of η_{SC}, as seen in Eq. (8), are plotted as a function of ΔE for such an emitter at T = 2000K. As a consequence of the competing demands mentioned above, η_{SC} peaks at a bandwidth of ~0.07 [eV]. This behavior is not at all unique to the emitter at 2000K. In fact, the optimal bandwidth is not particularly sensitive to emitter temperature, remaining roughly constant over the entire range of relevant STPV temperatures (1000-2500K). The important point here is that there is an optimal (non-zero) bandwidth regarding the emitter due to thermodynamic consideration in the solar cell [3]. To obtain high solar cell efficiency it is in fact *un-desirable* to have emitters with too narrow a bandwidth [3].

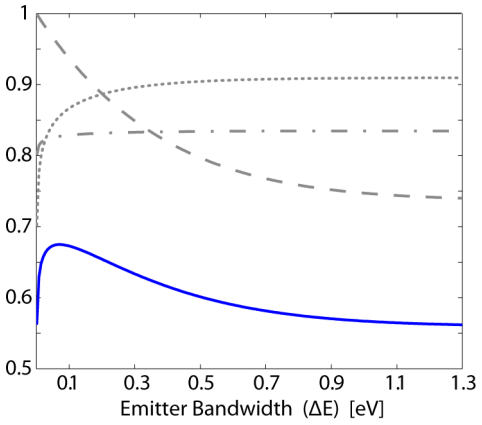

Fig. 4. Solar cell η_{SC} (blue curve) and its three components: $U\left(T,E_g\right)$ (dashed curve), $\upsilon\left(T,E_g\right)$ (dotted curve), and $m\left(V_{op}\right)$ (dashed-dotted curve), for the case of an idealized emitter at $T=2000K$ with emissivity: $\varepsilon_{ideal}\left(\Delta E\right)=\Theta\left(E-E_g\right)-\Theta\left(E-E_g-\Delta E\right)$ with $E_g=0.7[eV]$

3.3 Emitter design

Based on the requirements discussed above we now discuss our emitter design. Previous emitters have included 1D or 2D tungsten gratings [16,18–21], 3D tungsten photonic crystals [22] and 1D metallo-dielectric photonic crystals [23,24]. Here, we adopt and modify the emitter design concept as outlined in Ref [24], where an emitter is created by placing a multilayer dielectric stack near a unstructured Tungsten surface, with a cavity layer separating the dielectric stack from the Tungsten. The multilayer dielectric stack creates a stop band in which it exhibits strong reflection and low transmission. In this structure a sharp emissivity peak near the middle of the stop-band can be achieved, by matching the stacks' transmissivity to the metal slabs' absorptivity at the peak wavelength, and by choosing the appropriate width of the cavity layer such that a cavity resonance at the peak wavelength is formed between the dielectric stack and the Tungsten.

#112945 - $15.00 USD Received 16 Jun 2009; revised 20 Jul 2009; accepted 20 Jul 2009; published 11 Aug 2009

For our purposes here, however, further modification of the design in Ref [24]. is needed. First of all, for photons with energies in the vicinity of 0.7[eV], the Tungsten slab has a reflectivity of 0.85. While the use of a multilayer film with a matching reflectivity of 0.85 in the middle of the stop band indeed achieves a peak with unity emissivity, away from the resonant peak such a structure offers only limited suppression of emissivity. Also, as discussed in the previous section, instead of a narrow-band emitter with a single emissivity peak, it would be more beneficial to have a sharp cut-off in emissivity spectrum for energy lower than 0.7[eV], and a plateau with near-unity emissivity above 0.7[eV].

In our design, we place the resonant peak at the upper edge of the stop-band (Fig. 5), using the same reflectivity matching condition as discussed above. As a result, the emissivity makes a sharp transition at the upper edge of the stop-band–from near zero to a peak at 0.7[eV] with near-unity emissivity. The middle of the stack's stop-band now has a much higher reflectivity compared with the Tungsten, resulting in a greatly suppressed emissivity for the structure inside the stop-band as a whole. In addition, this design places the photonic stop-band entirely below the solar-cell band-gap of 0.7[eV]—where it is most needed. Below the stop-band $\left(E < 0.4[eV]\right)$ the emissivity oscillates with its maxima comparable to that of a tungsten slab. Nevertheless, the emissivity of the overall structure is low due to the low emissivity of tungsten, and the fact that the structure no longer satisfies the resonant condition that enhances emissivity. For a characteristic STPV temperature of 2000K the peak of the blackbody spectrum falls within the stop band. The emitter radiation in the energy range below the stop-band represents therefore only a small portion of the total radiative power. While such radiation, which is below solar cell band-gap, is a loss mechanism, its overall detrimental effect to the efficiency is relatively weak.

#112945 - $15.00 USD Received 16 Jun 2009; revised 20 Jul 2009; accepted 20 Jul 2009; published 11 Aug 2009

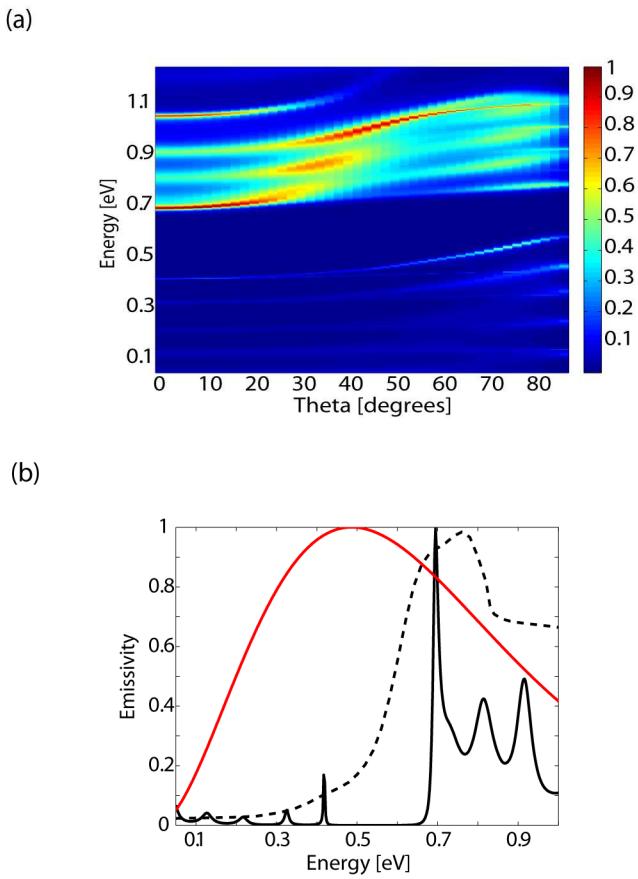

Fig. 5. Properties of the emitter, shown in Fig. 1(c), that consists of a Tungsten slab and a multilayer dielectric stack. (a) Emissivity (averaged over both polarizations) vs. polar angle and energy. (b) The black curve is the emissivity of our emitter structure at normal incidence ($\theta = 0$). The dashed black curve is the emissivity at normal incidence of a tungsten crossed grating structure ($1.5\mu m$ period; $1\mu m$ hole width; 400 nm hole depth). The red curve is the scaled spectral radiance of a 2000K blackbody.

Having presented the key design considerations and the end results above, we now provide some details on the design procedure for the dielectric stack. We started with a multi-layer stack consisting of 10 layers of alternating Si / SiO_2 on top of an unstructured tungsten slab (which can be thought of as the substrate of our tungsten absorber), with initial thicknesses for the Si / SiO_2 layers chosen to provide omni-directional reflection in the energy range directly below 0.7[eV], using the procedure outlined in [25]. Then, the multilayer dielectric stack was optimized (including the spacing between it and the tungsten slab) iteratively. At each iteration we picked several layers and varied their thickness randomly and independently. The emissivity spectrum of the resulting structure, over all angles and both polarizations, is then calculated using a scattering matrix formalism [26]. Using this emissivity spectrum, we then calculated the solar cell efficiency η_{SC} using the formulas in section 3.1. If a structure variation resulted in higher solar cell efficiency, such a variation was kept as the starting point for the next iteration. The optimization was run until the solar cell efficiency had saturated.

In simulating the emitter structures, we use the real and imaginary parts of the permittivity of Si, SiO_2, W as taken from [27]. Thus the simulation directly takes into account both the

#112945 - $15.00 USD Received 16 Jun 2009; revised 20 Jul 2009; accepted 20 Jul 2009; published 11 Aug 2009

dispersion and the loss of these material systems. In particular, although Si has a certain amount of loss at energies above 1.1[eV], in the relevant energy range for this analysis the structure has a negligible amount of absorption since its thickness is only a few microns. In fact, we have verified that loss in silicon contributes negligibly to the emitter's apparent emissivity by comparing our simulation result to the emissivity with Silicon's imaginary permittivity set to zero. Moreover, at high enough energies—where Si loss cannot be ignored—its effect is attenuated by the characteristic blackbody spectral radiance (see discussion in section 3.2).

Making use of our emitter's angular emissivity and the above SQ analysis in Section 3, we calculated the efficiency η_{SC} of a 0.7[eV] single-junction cell, as the temperature of the emitter is varied. As shown in Fig. 6(a), η_{SC} peaks at T = 2360K with a value of 50.8%, with the efficiency decreasing at lower temperatures due to increased sub-band-gap emission, and decreasing at higher temperatures due to increased above-band-gap emission that leads to thermalization losses.

Figure 5b provides a direct comparison between our multilayer design, with alternative emitter structures based on creating nanostructures directly within Tungsten without the use of an external dielectric multilayer structure. As an example, in Fig. 5(b) we plot the normal emissivity of a tungsten crossed-grating emitter consisting of a square lattice of square holes introduced in Tungsten slab. The lattice has a period of $1.5\mu m$. Each hole has a width of $1\mu m$ and a depth of $400nm$. While this choice of parameters leads to a peak with near-unity emissivity close to 0.7[eV], the width of this peak is much broader compared with our design shown in Fig. 5(b), with a much more gradual falling-off of emissivity at lower energies. In order to see the problem regarding such an emitter, we plot the emission spectrum of a blackbody at 2000K. Notice that the peak of the blackbody radiation is located at 0.5[eV]. The broad spectral peak of the crossed-grating structure thus provides limited suppression of sub-band-gap radiation. This is in fact a characteristic problem of most emitters.

4. System efficiency

We now consider a STPV system with a 0.7[eV] solar cell, utilizing the absorber designed in Section 2 and the emitter designed in Section 3. To obtain overall system efficiency, we multiply the solar cell efficiency η_{SC} as plotted in Fig. 6(a), with the absorber efficiency η_I as plotted in Fig. 2(b). The result, as plotted in Fig. 6(b), shows the overall system efficiency as a function of solar concentration and the equilibrium temperature of the intermediate. The efficiency is seen to achieve a maximum of ~50%. Moreover, the efficiency is shown to exceed the SQ limit of 41% over a wide range of intermediate temperatures (typically in the range of 1000-3000K), and a wide range of concentration values (typically in the range above 1000 suns and 1600 suns for ideal solar source and AM1.5 solar source, respectively.)

As a more detailed comparison in terms of efficiency between our designed STPV system and a single-junction cell, in Fig. 6(c) we plot the maximum efficiency of our designed STPV system and the solar cell directly exposed to sunlight as a function of solar concentration. For the STPV system, the maximum efficiency is obtained by choosing the equilibrium temperature that maximizes the system efficiency under a given concentration. For the solar cell, we consider two cases: the same 0.7[eV] cell as we use in the STPV system, and a 1.1[eV] cell–which is known in the SQ analysis to be the optimal band-gap, resulting in 41% efficiency for full concentration. We note that the STPV efficiency *surpasses the Shockley-Queisser limit of a single-junction cell*. In particular, even though practical intermediate temperature considerations effectively exclude using 1.1[eV] solar cells in STPV, it is possible to exceed the photovoltaic efficiency limit set by such cells using lower band-gap materials.

#112945 - $15.00 USD Received 16 Jun 2009; revised 20 Jul 2009; accepted 20 Jul 2009; published 11 Aug 2009

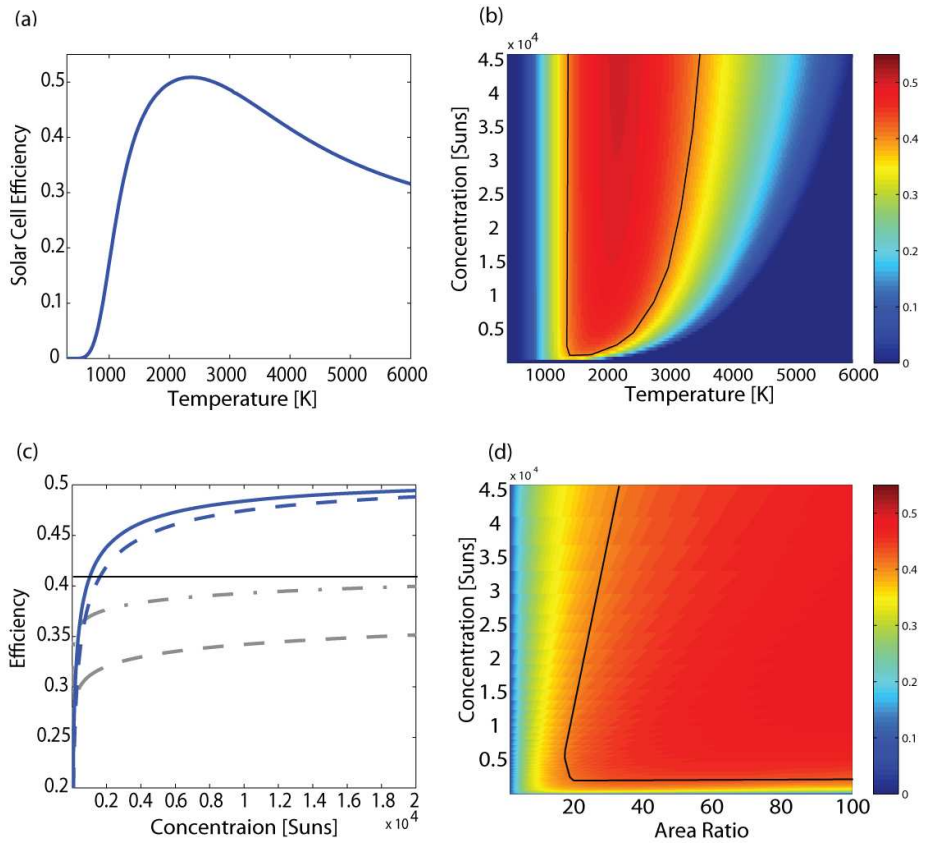

Fig. 6. (a) Efficiency η_{SC} of a 0.7[eV] solar cell exposed to radiation from our emitter shown in Fig. 1(c). (b) STPV system efficiency vs. temperature and concentration (black contour indicates the SQ limit at 41%.) (c) System efficiency vs. concentration, blue curve: maximum STPV system efficiency using our absorber and emitter pair and a 0.7[eV] solar cell (Ideal 6000K blackbody—solid line; AM 1.5 spectrum—dashed line); Grey curves: Dashed–efficiency of a 0.7[eV] cell; Dashed-dotted–efficiency of a 1.1[eV] cell, both when directly exposed to sunlight; Black line: theoretical limit of 41% in SQ analysis. (d) STPV system efficiency vs. area ratio and concentration (black contour indicates the SQ limit.)

In the above analysis we study the system efficiency as we vary the temperature of the intermediate. In practice, the intermediate temperature is set by choosing the area ratio between the absorber and the emitter, as seen in Eq. (1). Thus, in Fig. 6(d), we plot the STPV efficiency vs. concentration and area ratio. The efficiency is shown to exceed the Shockely-Queisser limit of 41% at an area ratio larger than ~16.

An area ratio of 16 as determined above should be reasonable to achieve in practice. (With a concentration of 1000 suns an intermediate with such an area ratio will reach an equilibrium temperature of ~2130K.) As an illustration, we consider an intermediate in a cylindrical geometry [13] (Fig. 7). At the center of the system is a Tungsten cylinder, with its top base patterned to create the absorber, and the side of the cylinder consisting of unstructured tungsten as in our emitter. The Tungsten cylinder is surrounded by the multilayer Si / SiO_2 structure to form the overall intermediate structure. In this setup the area ratio is proportional to the ratio between the height and radius of the cylinder. The intermediate is supported by an insulating rod, resulting in low heat conduction losses and thus allowing large area ratios.

#112945 - $15.00 USD Received 16 Jun 2009; revised 20 Jul 2009; accepted 20 Jul 2009; published 11 Aug 2009

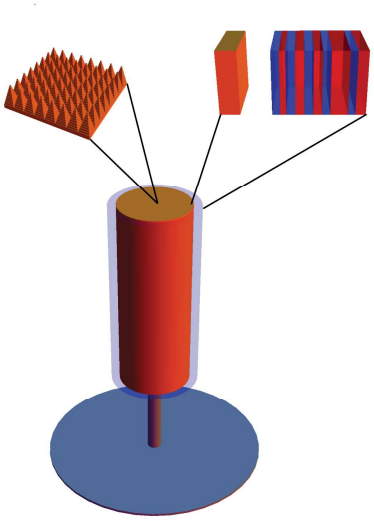

Fig. 7. Illustration of STPV intermediate in a cylindrical geometry. The cylinders' top base serves as absorber while its side serves as emitter. Magnifications show the systems' microscopic structure.

5. Conclusions

In this paper we presented an analysis of a STPV system with realistic nano-structured absorber and emitter pair. The absorber was designed to absorb solar light efficiently at all angles. The emitter was designed to have sharp sub-band-gap emissivity suppression at all emission angles, in addition to a narrow emissivity peak at the band-gap. The composite system was shown to surpass the SQ limit for sufficient light concentration, thus illustrating the practicality and potential usefulness of STPV systems with structured intermediates in providing efficient solar energy conversion.

Acknowledgments

This work is supported in part by the GCEP program at Stanford, and by an AFOSR-MURI program (FA9550-08-1-0407). E. R. acknowledges the support of the William R. and Sara Hart Kimball Stanford Graduate Fellowship. S. F. acknowledges discussions with Peter Peumans.

#112945 - $15.00 USD Received 16 Jun 2009; revised 20 Jul 2009; accepted 20 Jul 2009; published 11 Aug 2009